
Trajectory Based Simulations of Quantum-Classical Systems

S. Bonella, D. F. Coker, D. Mac Kernan, R. Kapral, and G. Ciccotti

¹ Dipartimento di Fisica, Università “La Sapienza”, Piazzale Aldo Moro, 2, 00185 Roma, Italy. sara.bonella@roma1.infn.it

² Department of Chemistry, Boston University, 590 Commonwealth Avenue, Boston, Massachusetts, 02215, U.S.A. and School of Physics, University College Dublin, Belfield, Dublin 4, Ireland coker@bu.edu

³ School of Physics, University College Dublin, Belfield, Dublin 4, Ireland. donal.mackernan@ucd.ie

⁴ Chemical Physics Theory Group, Department of Chemistry, University of Toronto, Toronto, Ontario M5S3H6, Canada rkapral@cptg.chem.utoronto.ca

⁵ Dipartimento di Fisica, Università “La Sapienza”, Piazzale Aldo Moro, 2, 00185 Roma, Italy giovanni.ciccotti@roma1.infn.it

Abstract. In this Chapter we review the core ingredients of a class of mixed quantum-classical methods that can naturally account for quantum coherence effects. In general, quantum-classical schemes partition degrees of freedom between a quantum subsystem and an environment. The various approaches are based on different approximations to the full quantum dynamics, in particular in the way they treat the environment. Here we compare and contrast two such methods: the Quantum Classical Liouville (QCL) approach, and the Iterative Linearized Density Matrix (ILDm) propagation scheme. These methods are based on evolving ensembles of surface-hopping trajectories in which the ensemble members carry weights and phases and their contributions to time-dependent quantities must be added coherently to approximate interference effects. The side by side comparison we offer highlights similarities and differences between the two approaches and serves as a starting point to explore more fundamental connections between such methods. The methods are applied to compute the evolution of the density matrix of a challenging condensed phase model system in which coherent dynamics plays a critical role: the asymmetric spin-boson. Various implementation questions are addressed.

1 Introduction

The difficulty in simulating the full quantum dynamics of large many-body systems has stimulated the development of mixed quantum-classical dynamical schemes. In such approaches, the quantum system of interest is partitioned into two subsystems, which we term the quantum subsystem, and quantum bath. Approximations to the full quantum dynamics are then made such that

the bath or environmental degrees of freedom are treated classically. The manner in which approximations are made to achieve this limit, and the resulting nature of the coupling between the quantum and classical subsystems distinguish the various quantum-classical schemes. While there are fundamental issues and difficulties that must be addressed when attempting to combine quantum and classical dynamics, quantum-classical schemes are, at present, the most useful and practical methods for treating realistic physical systems. A variety of such methods has been proposed [1, 2]. Some of the most popular quantum-classical methods are based on surface-hopping dynamics, where the system evolves classically on single adiabatic surfaces, with quantum transitions between these surfaces to account for nonadiabatic effects [3]. An important issue concerning the validity and implementation of surface-hopping schemes is the manner in which quantum coherence is treated.

In this chapter we describe two quantum-classical schemes that account for quantum coherence and involve simulations using ensembles of surface-hopping trajectories: the Quantum Classical Liouville (QCL) approach, and the iterative linearized density matrix (ILDm) propagation scheme. These methods are based on different approximations to the full quantum dynamics, in particular in the way they treat the environment. The QCL approach starts from an expansion of the quantum Liouville operator and develops approximate evolution equations for the density, while the ILDM approach employs a linearized path integral expression for the same quantity. Previous work has been done that begins to explore the relationship between these approaches [4] but more theoretical analysis is needed to understand the precise connection. In this chapter we present a side by side comparison of the two theoretical approaches, the algorithmic issues needed to implement them, and explore their performances on a common benchmark problem as a prelude for the analysis of this connection. Rather than give complete and detailed derivations of these two approaches, here we summarize the conceptual framework underlying the different methods and, where appropriate, point the reader to the original articles for complete details.

A complete and detailed analysis of the formal properties of the QCL approach [5] has revealed that while this scheme is internally consistent, inconsistencies arise in the formulation of a quantum-classical statistical mechanics within such a framework. In particular, the fact that time translation invariance and the Kubo identity are only valid to $\mathcal{O}(\hbar)$ have implications for the calculation of quantum-classical correlation functions. Such an analysis has not yet been conducted for the ILDM approach. In this chapter we adopt an alternative prescription [6, 7]. This alternative approach supposes that we start with the full quantum statistical mechanical structure of time correlation functions, average values, or, in general, the time dependent density, and develop independent approximations to both the quantum evolution, and to the equilibrium density. Such an approach has proven particularly useful in many applications [8, 9]. As was pointed out in the earlier publications [6, 7], the consistency between the quantum equilibrium structure and the approximate

dynamics is lost with such an approach, though we gain the ability explore different independent approximations to the evolution and the equilibrium structure.

The focus of this chapter is exploration of the ability of mixed quantum classical approaches to capture the effects of interference and coherence in the approximate dynamics used in these different mixed quantum classical methods. As outlined below, the expectation values of computed observables are fundamentally non-equilibrium properties that are not expressible as equilibrium time correlation functions. Thus, the chapter explores the relationship between the approximations to the quantum dynamics made in these different approaches that attempt to capture quantum coherence.

The main goal in the development of mixed quantum classical methods has as its focus the treatment of large, complex, many-body quantum systems. While applications to models with many realistic elements have been carried out [10,11], here we test the methods and algorithms on the spin-boson model, which is the standard test case in this field. In particular, we focus on the asymmetric spin-boson model and the calculation of off-diagonal density matrix elements, which present difficulties for some simulation schemes. We show that both of the methods discussed here are able to accurately and efficiently simulate this model.

The chapter is organized as follows: The quantum-classical Liouville dynamics scheme is first outlined and a rigorous surface hopping trajectory algorithm for its implementation is presented. The iterative linearized density matrix propagation approach is then described and an approach for its implementation is presented. In the Model Simulations section the comparable performance of the two methods is documented for the generalized spin-boson model and numerical convergence issues are mentioned. In the Conclusions we review the perspectives of this study.

2 Quantum-Classical Liouville Dynamics

In quantum-classical Liouville (QCL) dynamics the partition of the system into bath and subsystem is motivated by the observation that for many condensed phase processes it is essential to account for the quantum mechanical character of only a few light (characteristic mass m) degrees of freedom; the remaining heavy (characteristic mass M) degrees of freedom may be treated classically to a high degree of accuracy.

2.1 Evolution equation

In this scheme, for a system with hamiltonian \hat{H} , the starting point is the quantum Liouville equation for the density matrix, $\hat{\rho}(t)$,

$$\frac{\partial}{\partial t} \hat{\rho}(t) = -\frac{i}{\hbar} [\hat{H}, \hat{\rho}(t)]. \quad (1)$$

The quantum-classical Liouville equation is obtained from this equation by introducing scaled variables such that the characteristic momenta of the light and heavy degrees of freedom are comparable. This scaling introduces a small parameter $\mu = (m/M)^{1/2}$ in the equations of motion. Expansion of the quantum Liouville operator to $\mathcal{O}(\mu)$ yields the quantum-classical Liouville equation [2, 4, 12–20],

$$\begin{aligned} \frac{\partial \hat{\rho}_W(R, P, t)}{\partial t} &= -\frac{i}{\hbar} \left[\hat{H}_W(R, P), \hat{\rho}_W(R, P, t) \right] \\ &\quad + \frac{1}{2} (\{ \hat{H}_W(R, P), \hat{\rho}_W(R, P, t) \} - \{ \hat{\rho}_W(R, P, t), \hat{H}_W(R, P) \}) \\ &= -i \hat{\mathcal{L}} \hat{\rho}_W(R, P, t). \end{aligned} \quad (2)$$

The last line defines the mixed quantum-classical Liouville operator $\hat{\mathcal{L}}$. The W subscripts denote a partial Wigner transform of an operator or density matrix. The phase space variables of the bath are (R, P) and the partial Wigner transform of the total hamiltonian is given by,

$$\hat{H}_W(R, P) = \frac{P^2}{2M} + \frac{\hat{p}^2}{2m} + \hat{V}_W(\hat{q}, R), \quad (3)$$

where \hat{p} is the set of momentum operators for the quantum subsystem with coordinate operators \hat{q} , and $\hat{V}_W(\hat{q}, R)$ is the partial Wigner transform of the total potential energy operator of the system. As usual, square brackets denote quantum commutators and curly brackets denote Poisson brackets. Similarly, the quantum-classical Liouville equation of motion for an operator \hat{B} is

$$\frac{d\hat{B}_W(R, P, t)}{dt} = i \hat{\mathcal{L}} \hat{B}_W(R, P, t). \quad (4)$$

One noteworthy feature of Eqs. (2) and (4) is that they provide an exact quantum description for an arbitrary quantum subsystem bilinearly coupled to a quantum harmonic bath. Other aspects of this equation have been discussed previously in the literature [2, 5].

2.2 Simulation of expectation values

The expectation value of an operator \hat{B} is given by

$$\overline{B(t)} = \text{Tr} \hat{B} \hat{\rho}(t) = \text{Tr} \hat{B}(t) \hat{\rho}(0) = \text{Tr}' \int dR dP \hat{B}_W(R, P, t) \hat{\rho}_W(R, P). \quad (5)$$

In the last equality here we have introduced the partial Wigner transforms of the density matrix and operator. The prime on the trace indicates a trace over the subsystem degrees of freedom. All information on the quantum initial distribution is contained in $\hat{\rho}_W(R, P, 0)$. In the evaluation of this expression we assume that the time evolution of $\hat{B}_W(R, P, t)$ is given by Eq. (4). This

equation may be simulated in a variety of representations, using various algorithms [2, 21]. Here we focus on a representation in the adiabatic basis and a Trotter-based scheme which leads to a simulation algorithm involving an ensemble of surface-hopping trajectories [22].

Given that the total hamiltonian may be written as $\hat{H}_W = P^2/2M + \hat{h}_W(R)$, the adiabatic eigenfunctions $|\alpha; R\rangle$ are the solutions of the eigenvalue problem, $\hat{h}_W(R)|\alpha; R\rangle = E_\alpha(R)|\alpha; R\rangle$. In this adiabatic basis the quantum-classical Liouville operator has matrix elements [12],

$$\begin{aligned} i\mathcal{L}_{\alpha\alpha',\beta\beta'} &= (i\omega_{\alpha\alpha'} + iL_{\alpha\alpha'})\delta_{\alpha\beta}\delta_{\alpha'\beta'} - \mathcal{J}_{\alpha\alpha',\beta\beta'} \\ &\equiv i\mathcal{L}_{\alpha\alpha'}^0\delta_{\alpha\beta}\delta_{\alpha'\beta'} - \mathcal{J}_{\alpha\alpha',\beta\beta'}. \end{aligned} \quad (6)$$

Here $\omega_{\alpha\alpha'}(R) = (E_\alpha(R) - E_{\alpha'}(R))/\hbar$ and $iL_{\alpha\alpha'}$ is the Liouville operator that describes classical evolution determined by the mean of the Hellmann-Feynman forces corresponding to adiabatic states α and α' ,

$$iL_{\alpha\alpha'} = \frac{P}{M} \cdot \frac{\partial}{\partial R} + \frac{1}{2} \left(F_W^\alpha + F_W^{\alpha'} \right) \cdot \frac{\partial}{\partial P}, \quad (7)$$

where $F_W^\alpha = -\langle \alpha; R | \frac{\partial \hat{H}_W(\hat{q}, R)}{\partial R} | \alpha; R \rangle$ is the Hellmann-Feynman force for state α . The operator $\mathcal{J}_{\alpha\alpha',\beta\beta'}$ is responsible for nonadiabatic transitions and associated changes in the bath momentum and can be written as the sum of two terms,

$$\mathcal{J}_{\alpha\alpha',\beta\beta'} = J_{1\alpha\alpha',\beta\beta'} + J_{2\alpha\alpha',\beta\beta'}, \quad (8)$$

where

$$J_{1\alpha\alpha',\beta\beta'} = -(d_{\alpha\beta}\delta_{\alpha'\beta'} + d_{\alpha'\beta}^*\delta_{\alpha\beta}) \cdot \frac{P}{M}, \quad (9)$$

$$J_{2\alpha\alpha',\beta\beta'} = -\frac{1}{2} \left((E_\alpha - E_\beta)d_{\alpha\beta}\delta_{\alpha'\beta'} + (E_{\alpha'} - E_{\beta'})d_{\alpha'\beta'}^*\delta_{\alpha\beta} \right) \cdot \frac{\partial}{\partial P}, \quad (10)$$

and $d_{\alpha\beta}(R) = \langle \alpha; R | \frac{\partial}{\partial R} | \beta; R \rangle$ is the nonadiabatic coupling matrix element. The matrix elements of the quantum-classical propagator in the adiabatic basis are $(\exp(i\mathcal{L}t))_{\alpha\alpha',\beta\beta'}$. The superoperator notation involving pairs of quantum states can be eliminated by associating an index $s = \alpha\mathcal{N} + \alpha'$ with the pair $(\alpha\alpha')$, where $0 \leq \alpha, \alpha' < \mathcal{N}$ for an \mathcal{N} -state quantum subsystem [22]. The quantum-classical propagator then takes the form $(\exp(i\mathcal{L}t))_{ss'}$ where $i\mathcal{L}_{ss'} = i\mathcal{L}_s^0\delta_{ss'} - \mathcal{J}_{ss'}$.

Since the Liouville operator is time independent and commutes with itself we may write the propagator exactly as the product of N short time propagators as

$$(e^{i\mathcal{L}t})_{s_0 s_N} = \sum_{s_1 s_2 \dots s_{N-1}} \prod_{j=1}^N \left(e^{i\mathcal{L}(t_j - t_{j-1})} \right)_{s_{j-1} s_j}, \quad (11)$$

where $t_j = j\delta$ and $t = N\delta$. The propagator for each of the small time intervals $t_j - t_{j-1} = \delta$ may be computed by using a Trotter factorization as

$$\left(e^{i\mathcal{L}(t_j-t_{j-1})} \right)_{s_{j-1}s_j} \approx e^{i\mathcal{L}_{s_{j-1}}^0 \delta/2} \left(e^{-\mathcal{J}\delta} \right)_{s_{j-1}s_j} e^{i\mathcal{L}_{s_j}^0 \delta/2} + \mathcal{O}(\delta^3), \quad (12)$$

where we have used the fact that $i\mathcal{L}^0$ is diagonal in the adiabatic basis. The propagator $e^{i\mathcal{L}_s^0(t_j-t_{j-1})}$ can be written as the product of a phase factor and a classical evolution operator as [12]

$$\begin{aligned} e^{i\mathcal{L}_s^0(t_j-t_{j-1})} &= e^{i \int_{t_{j-1}}^{t_j} d\tau \omega_s(R_{s,\tau})} e^{iL_s(t_j-t_{j-1})} \\ &\equiv \mathcal{W}_s(t_{j-1}, t_j) e^{iL_s(t_j-t_{j-1})}, \end{aligned} \quad (13)$$

where $R_{s,\tau}$ denotes the value of R at time τ obtained by classical evolution under the Hellmann-Feynman force with quantum state index s .

The propagator $(e^{-\mathcal{J}\delta})_{ss'}$ is responsible for quantum transitions and bath momentum changes. In order to compute its action, we use the momentum-jump approximation [12, 23] that replaces the small continuous momentum changes with momentum jumps that accompany each quantum transition. In this approximation, the matrix elements of $e^{-\mathcal{J}\delta}$ can be written in terms of a matrix \mathcal{M} to $\mathcal{O}(\delta^2)$,

$$\left(e^{-\mathcal{J}\delta} \right)_{ss'} \approx (Q_1)_{ss'} e^{C_{ss'} \cdot \frac{\partial}{\partial P}} + \mathcal{O}(\delta^2) = \mathcal{M}_{ss'}(\delta) + \mathcal{O}(\delta^2). \quad (14)$$

The explicit forms of the Q_1 and C matrices may be written for any \mathcal{N} -state quantum system. For a two-level system they have the forms,

$$Q_1 = \begin{pmatrix} \cos^2(a) & -\cos(a)\sin(a) & -\cos(a)\sin(a) & \sin^2(a) \\ \sin(a)\cos(a) & \cos^2(a) & -\sin^2(a) & -\sin(a)\cos(a) \\ \sin(a)\cos(a) & -\sin^2(a) & \cos^2(a) & -\sin(a)\cos(a) \\ \sin^2(a) & \sin(a)\cos(a) & \sin(a)\cos(a) & \cos^2(a) \end{pmatrix}, \quad (15)$$

where $a = \frac{P}{M} \cdot d_{10}(R)\delta$ and

$$C = \begin{pmatrix} 0 & S_{01} & S_{01} & 2S_{01} \\ S_{10} & 0 & 0 & S_{01} \\ S_{10} & 0 & 0 & S_{01} \\ 2S_{10} & S_{10} & S_{10} & 0 \end{pmatrix}, \quad (16)$$

where $S_{\alpha\beta} = \hbar\omega_{\alpha\beta}d_{\alpha\beta}/(2(P/M) \cdot d_{\alpha\beta})$. The momentum jump operators can be evaluated as

$$\begin{aligned} e^{S_{\alpha\beta} \cdot \partial/\partial P} f(P) &= e^{\hbar\omega_{\alpha\beta}M\partial/\partial(\hat{d}_{\alpha\beta} \cdot P)^2} f \left(P_{\perp} + \hat{d}_{\alpha\beta} \text{sgn}(\hat{d}_{\alpha\beta} \cdot P) \sqrt{(\hat{d}_{\alpha\beta} \cdot P)^2} \right) \\ &= f(P + \Delta P_{\alpha\beta}). \end{aligned}$$

where

$$\Delta P_{\alpha\beta} = \hat{d}_{\alpha\beta} \left(\text{sgn}(\hat{d}_{\alpha\beta} \cdot P) \sqrt{(\hat{d}_{\alpha\beta} \cdot P)^2 + \hbar\omega_{\alpha\beta}M} - (\hat{d}_{\alpha\beta} \cdot P) \right) \quad (17)$$

and P has been decomposed into its components along and normal to $\hat{d}_{\alpha\beta}$ as $P = (1 - \hat{d}_{\alpha\beta}\hat{d}_{\alpha\beta}) \cdot P + \hat{d}_{\alpha\beta}(\hat{d}_{\alpha\beta} \cdot P) \equiv P_{\perp} + \hat{d}_{\alpha\beta}(\hat{d}_{\alpha\beta} \cdot P) = P_{\perp} + \hat{d}_{\alpha\beta}\text{sgn}(\hat{d}_{\alpha\beta} \cdot P) \sqrt{(\hat{d}_{\alpha\beta} \cdot P)^2}$.

Using these expressions in the Trotter expansion (12) we obtain

$$\begin{aligned} \left(e^{i\mathcal{L}(t_j - t_{j-1})} \right)_{s_{j-1}s_j} &\approx e^{i\mathcal{L}_{s_{j-1}}^0 \delta/2} \mathcal{M}_{s_{j-1}s_j}(\delta) e^{i\mathcal{L}_{s_j}^0 \delta/2} \\ &= \mathcal{W}_{s_{j-1}}(t_{j-1}, t_j - \delta/2) e^{iL_{s_{j-1}} \delta/2} \mathcal{M}_{s_{j-1}s_j}(\delta) \mathcal{W}_{s_j}(t_j - \delta/2, t_j) e^{iL_{s_j} \delta/2}. \end{aligned} \quad (18)$$

From left to right, the short-time propagator describes classical propagation on the s_{j-1} surface through a time interval $\delta/2$, a transition $s_{j-1} \rightarrow s_j$ determined by the elements of \mathcal{M} and classical propagation on the s_j surface for a time interval $\delta/2$.

Short time segments may be concatenated to obtain the time evolution for any time. Using Eq. (18), we may write the expression for $\overline{B(t)}$ more explicitly as

$$\begin{aligned} \overline{B(t)} &= \sum_{s_0} \int dRdP B_W^{s_0}(R, P, t) \rho_W^{s'_0}(R, P) dRdP \\ &= \sum_{s_0} \int \rho_W^{s'_0}(R, P) \sum_{s_1, \dots, s_N} \left[\prod_{j=1}^N \mathcal{W}_{s_{j-1}}(t_{j-1}, t_j - \delta/2) e^{iL_{s_{j-1}} \delta/2} \right. \\ &\quad \left. \times \mathcal{M}_{s_{j-1}s_j}(\delta) \mathcal{W}_{s_j}(t_j - \delta/2, t_j) e^{iL_{s_j} \delta/2} \right] B_W^{s_N}(R, P), \end{aligned} \quad (19)$$

where $s'_0 = (\alpha'_0, \alpha_0)$ is obtained from $s_0 = (\alpha_0, \alpha'_0)$ by the interchange $\alpha_0 \rightleftharpoons \alpha'_0$. The summations on quantum indices and phase space integrals can be performed through Monte Carlo sampling. The simulation algorithm consists of three steps based on the structure of Eq. (19). The total time of the simulation is divided into $t/\delta = N$ short time segments. Given the form of the short time propagator in Eq. (18) we can rearrange Eq. (19) into the form

$$\begin{aligned} \overline{B(t)} &= \frac{\mathcal{N}^2}{K} \sum_{\kappa=1}^K \frac{\rho_W^{s'_0 \kappa}(R^\kappa, P^\kappa)}{|\rho_W^{s_0 \kappa}(R^\kappa, P^\kappa)|} \left[\prod_{j=1}^N \left(\mathcal{W}_{s_{j-1}^\kappa}(t_{j-1}, t_j - \delta/2) e^{iL_{s_{j-1}^\kappa} \delta/2} \right. \right. \\ &\quad \left. \left. \times \frac{\sum_{s_j^\kappa} |(Q_1)_{s_{j-1}^\kappa s_j^\kappa}(\delta)|}{|(Q_1)_{s_{j-1}^\kappa s_j^\kappa}(\delta)|} \mathcal{M}_{s_{j-1}^\kappa s_j^\kappa}(\delta) \mathcal{W}_{s_j^\kappa}(t_j - \delta/2, t_j) e^{iL_{s_j^\kappa} \delta/2} \right)_{s_{j-1}^\kappa s_j^\kappa} \right] \\ &\quad \times B_W^{s_N \kappa}(R^\kappa, P^\kappa), \end{aligned} \quad (20)$$

that can be evaluated by Monte Carlo sampling. Here the index κ refers to the Monte Carlo sampling of the elementary event $(R^\kappa, P^\kappa, s_0^\kappa, s_1^\kappa, \dots, s_N^\kappa)$,

and results are averaged over K such events. The \mathcal{N}^2 factor arises from the uniform sampling for the sum on the initial states s_0 . Phase space is importance sampled according to $|\rho_W^{s'_0}(R, P)|$, which leaves in the sum the phase factor, $\sigma = \rho_W^{s'_0}(R, P)/|\rho_W^{s'_0}(R, P)|$.

Evaluation of Eq. (20) involves a combination of Monte Carlo sampling and propagation steps. For ($j = 1$) the phase space point (R, P) is propagated classically to $e^{iL_{s_0}\delta/2}(R, P) = (R', P')$. The phase factor \mathcal{W}_{s_0} and all of the matrix elements and operators, including the observable, at the value of this evolved phase point, are updated. The value of the index s_1 in the matrix $\mathcal{M}_{s_0 s_1}(\delta)$ is chosen by sampling with probability $|(Q_1)_{s_0 s_1}(\delta)|/\sum_{s_1} |(Q_1)_{s_0 s_1}(\delta)|$. This introduces the factor $\sum_{s_1} |(Q_1)_{s_0 s_1}(\delta)|/|\sum_{s_1} |(Q_1)_{s_0 s_1}(\delta)|$. Once the index s_1 is selected, the momentum jump (if any) specified by $\mathcal{M}_{s_0 s_1}(\delta)$ is applied to all functions and operators to its right so that the new bath phase space point is (R', \bar{P}') , where the overline denotes the momentum after the momentum-jump operation. The phase factor \mathcal{W}_{s_1} is then computed and the evolution operator $e^{iL_{s_1}\delta/2}$ is used to propagate the bath phase space coordinates (R', \bar{P}') to time t_1 : $e^{iL_{s_1}\delta/2}(R', \bar{P}') = (R'', P'')$. The procedure is then repeated starting from the index $j = 2$ in the product in Eq. (20) with the updated value of the bath phase space point.

An important additional part of the algorithm is the use of a filter. Estimates of averages are dominated by large fluctuations which come from unusually large values of the summand of Eq. (20) and exacerbate the sign problem that comes from the phase factors in the evolution. The use of a filter can eliminate improperly large biasing fluctuations which should not contribute to the averaged quantity. A simple filter involves putting an upper bound, Z , on the magnitude of the factor in the square brackets appearing in the summand in Eq. (20). When, at step j in the calculation of the product in the summand, the running summand exceeds the bound, the factor in the updating of the running product is put to unity and the index s_j is set to s_{j-1} . The reader can find details of this approach in reference [10, 22].

3 Iterative Linearized Density Matrix Propagation

Rather than starting from the exact quantum Liouville equation for the density matrix and approximating it by the mixed quantum-classical Liouville equation as in the QCL scheme outlined above, the iterative linearized density matrix propagation approach, in contrast, starts from an exact expression for the evolution of the density operator and then uses the time composition property of the quantum propagators to write this evolution in terms of concatenated time segments. In much the same way as with the formal development of path integral expressions, a short time approximation for the propagating density matrix in each segment is developed. With in each individual time segment evolution occurs according to the prescriptions of the

linearized approximation as outlined in the literature [24–28]. The basic idea behind this alternative approximate scheme is that, for sufficiently short times, the forward and backward paths of the environmental degrees of freedom that are used to represent the evolving density matrix must remain close to one another. Truncating an expansion in the difference between forward and backward paths for these degrees of freedom at linear order should provide a good short time approximation. With this approach, contributions from forward and backward paths of the quantum subsystem degrees of freedom are included to all orders. The time segments in the iterative implementation of this short time approximation are joined by a stochastic mechanism that samples the relevant contributions to the evolving density matrix at any given time. Thus, linearization becomes a tool to obtain a satisfactory approximation for a sequence of propagators in the spirit of a “finite time” path integral expression for the density operator in which the length of the “time slices” is not necessarily infinitesimal. Since the approximations underlying the linearized expression for the propagators are more accurate for short times, the performance of the overall dynamics is expected to improve with the number of time slices. During each individual propagation leg, non adiabaticity is described through the evolution of quantum amplitudes represented in the mapping formulation [29–33]. At the end of each finite time slice, the quantum subsystem representation is refreshed by a Monte Carlo selection of the most important term in the density matrix at that particular time in a similar fashion to that outlined in the previous section. In the following we summarize the results needed to derive the approach and present an algorithm that combines evolution of classical trajectories and Monte Carlo sampling to implement the theory.

3.1 Theory

The time evolution of density operator $\hat{\rho}(t)$ in the Heisenberg picture is given by

$$\hat{\rho}(t = n\Delta) = e^{-\frac{i}{\hbar}\hat{H}\Delta} \dots e^{-\frac{i}{\hbar}\hat{H}\Delta} \hat{\rho}(0) e^{\frac{i}{\hbar}\hat{H}\Delta} \dots e^{\frac{i}{\hbar}\hat{H}\Delta} \quad (21)$$

where, to set the stage for the approach to be described, the total time propagation to t has been broken up into n time intervals of finite duration Δ .

Inserting resolutions of the identity written in terms of tensor product states $|R_{j\Delta}\alpha_{j\Delta}\rangle$ (with $0 \leq j \leq (n - 1)$) in the coordinate and diabatic state representation, matrix elements of the time dependent density operator are conveniently written as

$$\begin{aligned}
& \langle R_{n\Delta} \alpha_{n\Delta} | \hat{\rho}(n\Delta) | R'_{n\Delta} \alpha'_{n\Delta} \rangle = \\
& \sum_{\alpha_{(n-1)\Delta}, \alpha'_{(n-1)\Delta}} \int dR_{(n-1)\Delta} dR'_{(n-1)\Delta} \cdots \sum_{\alpha_0, \alpha'_0} \int dR_0 dR'_0 \\
& \times \langle R_{n\Delta} \alpha_{n\Delta} | e^{-\frac{i}{\hbar} \hat{H} \Delta} | R_{(n-1)\Delta} \alpha_{(n-1)\Delta} \rangle \cdots \langle R_{\Delta} \alpha_{\Delta} | e^{-\frac{i}{\hbar} \hat{H} \Delta} | R_0 \alpha_0 \rangle \\
& \times \langle R_0 \alpha_0 | \hat{\rho}(0) | R'_0 \alpha'_0 \rangle \\
& \times \langle R'_0 \alpha'_0 | e^{\frac{i}{\hbar} \hat{H} \Delta} | R'_{\Delta} \alpha'_{\Delta} \rangle \cdots \langle R'_{(n-1)\Delta} \alpha'_{(n-1)\Delta} | e^{\frac{i}{\hbar} \hat{H} \Delta} | R'_{n\Delta} \alpha'_{n\Delta} \rangle
\end{aligned} \tag{22}$$

In this expression, each individual sum extends over all the \mathcal{N} diabatic basis states.

A convenient expression for the incremental time evolution of the density matrix in the time interval $0 \leq \tau \leq \Delta$, for example, can be obtained as described in detail in references [34–36]. Briefly, a hybrid coordinate-momentum path integral representation of the forward and backward propagators for the environmental degrees of freedom is introduced, together with the mapping hamiltonian representation of the evolution of the quantum subsystem [29–33]. The latter can be evaluated explicitly and exactly as a parametric function of the paths of the bath variables by averaging the contributions of a set of auxiliary classical trajectories for the mapping variables $(p_{\tau, \lambda}, q_{\tau, \lambda})$ obtained by solving the following equations:

$$\begin{aligned}
\dot{q}_{\tau, \lambda} &= h_{\lambda, \lambda}(R_{\tau}) p_{\tau, \lambda} + \sum_{\mu \neq \lambda} h_{\lambda, \mu}(R_{\tau}) p_{\tau, \mu} \\
\dot{p}_{\tau, \lambda} &= -h_{\lambda, \lambda}(R_{\tau}) q_{\tau, \lambda} - \sum_{\mu \neq \lambda} h_{\lambda, \mu}(R_{\tau}) q_{\tau, \mu}
\end{aligned} \tag{23}$$

Here $h_{\lambda, \mu}(R_{\tau})$ is the matrix element of the quantum subsystem hamiltonian in the diabatic basis, including its interaction with the environment (see reference [37] for details). These manipulations transform the integrand in Eq. (22) into an explicit complex function of the bath and mapping variables. A change of variables is introduced that transforms the integration over forward, R_{τ} , and backward, R'_{τ} environmental paths into integration over the mean $\bar{R}_{\tau} = (R_{\tau} + R'_{\tau})/2$ and difference paths $Z_{\tau} = (R_{\tau} - R'_{\tau})$. The total phase of the new path integral expression is then expanded to linear order in the bath difference path. This approximation makes it possible to evaluate all difference integrals analytically to arrive at the following result for the reduced density matrix elements for the first time increment Δ which is divided into K discrete environmental path integral time steps of duration δ , *i.e.* $\Delta = K\delta$.

$$\begin{aligned}
 \langle \bar{R}_K + \frac{Z_K}{2} \alpha_\Delta | \hat{\rho}(\Delta) | \bar{R}_K - \frac{Z_K}{2} \alpha'_\Delta \rangle = & \\
 \sum_{\alpha_0, \alpha'_0} \int d\bar{R}_0 dq_0 dp_0 dq'_0 dp'_0 r'_{0, \alpha'_0} e^{-i\Theta'_{0, \alpha'_0}} G'_0 r_{0, \alpha_0} e^{i\Theta_{0, \alpha_0}} G_0 & \\
 \times \int \prod_{k=1}^{K-1} d\bar{R}_k \frac{d\bar{P}_k}{2\pi} \frac{d\bar{P}_K}{2\pi} [\hat{\rho}]_W^{\alpha_0, \alpha'_0}(\bar{R}_0, \bar{P}_1) e^{i\bar{P}_K Z_K} & \quad (24) \\
 \times r_{\Delta, \alpha_\Delta}(\{\bar{R}_k\}) r'_{\Delta, \alpha'_\Delta}(\{\bar{R}_k\}) e^{-i\delta \sum_{k=1}^K (\theta_{\alpha_\Delta}(\bar{R}_k) - \theta_{\alpha'_\Delta}(\bar{R}_k))} & \\
 \times \prod_{k=1}^{K-1} \delta \left(\frac{\bar{P}_{k+1} - \bar{P}_k}{\delta} - F_k^{\alpha_\Delta, \alpha'_\Delta} \right) \prod_{k=1}^K \delta \left(\frac{\bar{P}_k}{M} - \frac{\bar{R}_k - \bar{R}_{k-1}}{\delta} \right) &
 \end{aligned}$$

here, the notation $\delta(\cdot)$ in the last line of Eq.(24) is the Dirac δ -function, $G_0 = e^{-\frac{1}{2} \sum_\lambda (q_{0,\lambda}^2 + p_{0,\lambda}^2)}$, $r_{\Delta, \alpha_\Delta}(\{\bar{R}_k\}) = \sqrt{q_{\Delta, \alpha_\Delta}^2(\{\bar{R}_k\}) + p_{\Delta, \alpha_\Delta}^2(\{\bar{R}_k\})}$, and

$$\begin{aligned}
 \Theta_{\Delta, \alpha_\Delta}(\{\bar{R}_k\}) = \tan^{-1} \left(\frac{p_{0, \alpha_\Delta}}{q_{0, \alpha_\Delta}} \right) + \int_0^\Delta d\tau h_{\alpha_\Delta, \alpha_\Delta}(R_\tau) & \\
 + \int_0^\Delta d\tau \sum_{\lambda \neq \alpha_\Delta} \left[h_{\alpha_\Delta, \lambda}(R_\tau) \frac{(p_{\tau \alpha_\Delta} p_{\tau \lambda} + q_{\tau \alpha_\Delta} q_{\tau \lambda})}{(p_{\tau \alpha_\Delta}^2 + q_{\tau \alpha_\Delta}^2)} \right] & \\
 = \tan^{-1} \left(\frac{p_{0, \alpha_\Delta}}{q_{0, \alpha_\Delta}} \right) + \int_0^\Delta \theta_{\alpha_\Delta}(R_\tau) d\tau & \quad (25)
 \end{aligned}$$

The partial Wigner transform of the initial density matrix element (2nd line of Eq.(24)) is

$$(\hat{\rho})_W^{\alpha_0, \alpha'_0}(\bar{R}_0, \bar{P}_1) = \int dZ_0 \langle \bar{R}_0 + \frac{Z_0}{2} \alpha_0 | \hat{\rho} | \bar{R}_0 - \frac{Z_0}{2} \alpha'_0 \rangle e^{-\frac{i}{\hbar} \bar{P}_1 Z_0} \quad (26)$$

and the “force” is

$$\begin{aligned}
 F_k^{\alpha_\Delta, \alpha'_\Delta} = -\frac{1}{2} \{ \nabla_{\bar{R}_k} h_{\alpha_\Delta, \alpha_\Delta}(\bar{R}_k) + \nabla_{\bar{R}_k} h_{\alpha'_\Delta, \alpha'_\Delta}(\bar{R}_k) \} & \quad (27) \\
 -\frac{1}{2} \sum_{\lambda \neq \alpha_\Delta} \nabla_{\bar{R}_k} h_{\alpha_\Delta, \lambda}(\bar{R}_k) \left\{ \frac{(p_{\alpha_\Delta k} p_{\lambda k} + q_{\alpha_\Delta k} q_{\lambda k})}{(p_{\alpha_\Delta k}^2 + q_{\alpha_\Delta k}^2)} \right\} & \\
 -\frac{1}{2} \sum_{\lambda \neq \alpha'_\Delta} \nabla_{\bar{R}_k} h_{\alpha'_\Delta, \lambda}(\bar{R}_k) \left\{ \frac{(p'_{\alpha'_\Delta k} p'_{\lambda k} + q'_{\alpha'_\Delta k} q'_{\lambda k})}{(p'^2_{\alpha'_\Delta k} + q'^2_{\alpha'_\Delta k})} \right\} &
 \end{aligned}$$

A detailed description of the derivation of these results can be found in references [34, 36].

Using Eq.(24) in Eq.(22) gives the iterative scheme developed in reference [37].

3.2 Implementation

In the iterative scheme outlined above, the evolution of all degrees of freedom has been reduced to classical trajectory propagation that can be efficiently performed. However, the number of terms included in the multiple sums in Eq. (22) grows exponentially with the number of time segments. This exponential growth can be controlled using an importance sampled Monte Carlo approach (see step (3) below). This involves implementing a trajectory surface hopping -like technique similar to that adopted in Ref. [39] and outlined under Eq. (20) above. The Monte Carlo induces hops between density matrix elements, *i.e.* pairs of state labels, and generates dynamical information about both populations (diagonal elements of the density matrix) and coherences (off-diagonal density matrix elements).

To demonstrate the algorithm let us consider two segments. There are five relevant times or time intervals:

(1) $\tau = 0$: The sum over initial quantum states α_0, α'_0 is performed explicitly. For each pair of initial quantum states selected, initial conditions for the bath variables are sampled from a probability density derived from the partial Wigner transform $[\hat{\rho}]_W^{\alpha_0, \alpha'_0}$ [25, 38]. The initial conditions for the mapping variables are specified by focusing on the occupied states for the forward and backward propagation [33, 37]. This initializes the occupied state mapping variables at the phase space point $(p_{\alpha_0}^o, q_{\alpha_0}^o) = (1/\sqrt{2}, 1/\sqrt{2})$, while the unoccupied state mapping variables originate from $(p_{\alpha_0}^u, q_{\alpha_0}^u) = (0, 0)$ (a similar set of conditions, with reversed initial momentum, is used to propagate the mapping variables in the backward propagator).

(2) $\tau \in (0, \Delta)$: The forces that evolve the initial conditions specified in (1), $F^{\alpha_\Delta, \alpha'_\Delta}$, depend on the labels of the quantum states at the end of the first time segment. According to Eq. (22) we must sum over all these labels as the starting states for the second propagation leg. Our approach thus generates $\mathcal{N} \times \mathcal{N} = \mathcal{N}_\rho$ trajectories, each governed by a different force $F^{\alpha_\Delta, \alpha'_\Delta}$, for the first propagation leg. The characteristics of the individual trajectories depend on the pair of indexes selected as the final quantum states and on the coupling between the electronic states during the propagation. In particular, if $\alpha_\Delta = \alpha'_\Delta$, Eq. (27) induces evolution on a single diabatic surface (first term on the right hand side) modulated by the coupling matrix elements and the mapping variables (second and third terms). On the other hand, if $\alpha_\Delta \neq \alpha'_\Delta$, the first term in the definition of the force amounts to propagation on a mean surface, while the second and third terms include modulation from couplings and mapping evolution as in the previous situation. Along the trajectories, the polynomial phase weights $r_{\Delta, \alpha_\Delta} r'_{\Delta, \alpha'_\Delta} \exp[-i \int_0^\Delta d\tau (\theta_{\alpha_\Delta}(\tau) - \theta_{\alpha'_\Delta}(\tau))]$ estimate the contributions of the different evolutions to the various density matrix elements. Note that, due to the focusing, initially occupied states start with weight equal to one, while unoccupied states begin with zero weight. These weights change, in the presence of couplings between the electronic

states, due to the amplitude transfer described by the evolution of the mapping variables.

(3) $\tau = \Delta$: At the end of the first segment, the \mathcal{N}_ρ trajectories have moved to different bath and mapping phase space points. In order to propagate the next leg we should, for each final point, propagate a new set of \mathcal{N}_ρ trajectories that experience different forces $F^{\alpha_{2\Delta}, \alpha'_{2\Delta}}$. If we were to propagate all these alternatives, the number of trajectories would grow as \mathcal{N}_ρ^σ where there are σ trajectory segments. To tame the exponential growth of the number of trajectories we implement a Monte Carlo (MC) procedure that substitutes the brute force sum over the quantum states at the intermediate time points along the propagation with an importance sampling of the different terms contributing to the value of the density matrix at the given time. The approach exploits the observation that during a given trajectory segment many of the quantum amplitudes that start out at zero at the beginning of the segment, remain very small at the end of the segment and this results in small polynomial weights and therefore small contributions to the integrals in Eq. (22). An MC branching procedure, whose probability distribution is based on the change in the quantum amplitudes during the current segment, is then used to decide which term in the double sum over states at the intermediate time is the most important. Thus, at the end of the first segment we compute the magnitudes of the contribution of the particular initial phase space point $(R_0, P_1, \alpha_0, \alpha'_0)$ to the density matrix elements for the new time, Δ , when this point has evolved to the \mathcal{N}_ρ final points $(R_K^{(\alpha_\Delta, \alpha'_\Delta)}, P_K^{(\alpha_\Delta, \alpha'_\Delta)}, \alpha_\Delta, \alpha'_\Delta)$ under the influence of the different forces $F^{\alpha_\Delta, \alpha'_\Delta}$. As described above, the magnitudes of these different contributions are $r_{\Delta, \alpha_\Delta} r'_{\Delta, \alpha'_\Delta}$, so we define the normalized probability distribution

$$M_{\alpha_\Delta, \alpha'_\Delta} = r_{\Delta, \alpha_\Delta} r'_{\Delta, \alpha'_\Delta} / \eta(\Delta) \quad (28)$$

with $\eta(\Delta) = \sum_{\alpha_\Delta, \alpha'_\Delta} r_{\Delta, \alpha_\Delta} r'_{\Delta, \alpha'_\Delta}$. We define the cumulative probabilities $C_{\beta_\Delta, \beta'_\Delta} = \sum_{\alpha_\Delta=1}^{\beta_\Delta} \sum_{\alpha'_\Delta=1}^{\beta'_\Delta} M_{\alpha_\Delta, \alpha'_\Delta}$. A uniform random number ξ on the interval $(0 < \xi < 1)$ is then selected. If the cumulative probability first becomes larger than ξ for indexes $\beta_\Delta = \alpha_\Delta^*$ and $\beta'_\Delta = \alpha'_\Delta^*$, the trajectory segment generated with forces $F^{\alpha_\Delta^*, \alpha'_\Delta^*}$ which evolves the density matrix from (α_0, α'_0) to $(\alpha_\Delta^*, \alpha'_\Delta^*)$ over the current segment is used as the MC sampled representative for the double sum $\sum_{\alpha_\Delta, \alpha'_\Delta}$ in Eq. (22). Since the Monte Carlo branching process is normalized by dividing by $\eta(\Delta)$ we must multiply out this time dependent normalization to preserve the true weight of the sampled trajectory segment. The sampled trajectory segment thus carries a weight and phase factor $\eta(\Delta) \exp[-i \int_0^\Delta d\tau (\theta_{\alpha_\Delta}(\tau) - \theta_{\alpha'_\Delta}(\tau))]$ which multiplies its contributions to the ensemble averages. Once the new pair of quantum state labels $(\alpha_\Delta^*, \alpha'_\Delta^*)$ is selected, the integrals over the corresponding mapping variables are again performed by focusing and this may introduce discontinuities in the polynomial weights and in the forces acting on the bath variables.

(4) $\tau \in (\Delta, 2\Delta)$: The new propagation segment evolves as in (2) with forces $F^{\alpha_{2\Delta}, \alpha'_{2\Delta}}$.

(5) $\tau = 2\Delta$: At the final time of the propagation, the “measurement” time, the overall weight of each contribution to the Monte Carlo in the initial conditions and state labels is computed. In the case of two segments, this is given by $\eta(\Delta) \exp[-i \int_0^\Delta d\tau (\theta_{\alpha_\Delta}(\tau) - \theta_{\alpha'_\Delta}(\tau))] r_{2\Delta, \alpha_{2\Delta}} r'_{2\Delta, \alpha'_{2\Delta}} \exp[-i \int_\Delta^{2\Delta} d\tau (\theta_{\alpha_{2\Delta}}(\tau) - \theta_{\alpha'_{2\Delta}}(\tau))]$. The different elements of the evolved density matrix can be evaluated by averaging these contributions over a set of repetitions of the Monte Carlo (and molecular dynamics) procedure described in (1)-(4).

The approach outlined above can be immediately generalized to the case of n propagation segments simply by iterating points (3) and (4). In this case, the weight at the final time $n\Delta$ becomes

$$\Omega_n = \left\{ \prod_{k=1}^{n-1} \eta(k\Delta) \exp[-i \int_{(k-1)\Delta}^{k\Delta} d\tau (\theta_{\alpha_{k\Delta}}(\tau) - \theta_{\alpha'_{k\Delta}}(\tau))] \right\} \\ \times r_{n\Delta, \alpha_{n\Delta}} r'_{n\Delta, \alpha'_{n\Delta}} \exp[-i \int_{(n-1)\Delta}^{n\Delta} d\tau (\theta_{\alpha_{n\Delta}}(\tau) - \theta_{\alpha'_{n\Delta}}(\tau))] \quad (29)$$

The combination of these phase factors and the weights that come from renormalizing after implementing the Monte Carlo density matrix element sampling lead to the same sorts of statistical convergence problems observed with the QCL implementation. Filtering techniques have not been implemented in these ILDM calculations so far, however, an approach inspired by the method outlined at the end of section 2 could be used to mitigate these convergence difficulties that can be particularly serious at longer times.

4 Model Simulations

In this section we present results using the two approaches described in the previous sections: the Trotter factorized QCL (TQCL), and iterative linearized density matrix (ILDM) propagation schemes, to study the spin-boson model consisting of a two level system that is bi-linearly coupled to a bath with M_h harmonic modes. This popular model of a quantum system embedded in an environment is described by the following general hamiltonian:

$$\hat{H} = \frac{1}{2} \sum_{j=1}^{M_h} (\hat{P}_j^2 + \omega_j^2 \hat{R}_j^2) + \epsilon \hat{\sigma}_z + \hat{\sigma}_z \sum_{j=1}^{M_h} g_j \hat{R}_j - \Omega \hat{\sigma}_x \quad (30)$$

where mass scaled coordinates have been used for the bath. We choose the couplings, g_j , and mode frequencies, ω_j , to be consistent with the exponentially truncated ohmic spectral density model for which the spectral density is $J(\omega) = \xi \omega e^{-\omega/\omega_c}$ [34, 39], where ξ is the friction or Kondo parameter and ω_c is the peak frequency in the spectral density. All the calculations outlined below

employ 20 bath modes coupled to the two level spin system. In this model hamiltonian Ω is the off-diagonal coupling strength between the two diabatic states of the quantum subsystem, and the parameter ϵ controls the asymmetry in energy between these states. This term acts like a “driving force” when the spin-boson model is applied to study charge transfer reactions in solution.

As noted earlier, the fundamental equations of the QCL dynamics approach are exact for this model, however, in order to implement these equations in the approach detailed in section 2 the momentum jump approximation of Eq.(14) is made in addition to the Trotter factorization of Eq.(12). Both approximations become more accurate as the size of the time step δ is reduced. Consequently, the results presented below primarily serve as tests of the validity and utility of the momentum-jump approximation. For a discussion of other simulation schemes for QCL dynamics see Ref. [21] in this volume. The linearized approximate propagator is not exact for the spin-boson model. However when used as a short time approximation for iteration as outlined in section 3 the approach can be made accurate with a sufficient number of iterations [37].

Figure 1 presents results for the time dependence of the diabatic state population difference, $\bar{B}(t) = \langle \sigma_z \rangle(t)$, for the symmetric spin-boson model ($\epsilon = 0$) for two interesting sets of conditions corresponding to low temperature-low friction, and intermediate temperature-high friction cases (see captions for details). Results from calculations employing the approximate methods outlined above are compared with exact benchmark results. Generally the agreement between results from the different approaches is quite reasonable though some systematic differences are apparent. The results obtained with the TQCL approach for the low temperature - low friction conditions show coherent population oscillations that have a slightly higher frequency and a slower decay than those obtained with the ILDM propagation scheme which generally show very good agreement with the exact results under these conditions. Much smaller differences between the various results are found at higher temperatures and frictions. The results presented here are converged with Trotter timestep (TQCL), number of attempted hops (ILDM), and ensemble size. Given that the QCL formulation should be exact for the spin-boson model the systematic differences observed in the low temperature-low friction results for TQCL approach can be attributed to the momentum-jump approximation that is made when implementing the formulation. This approximation seems to have the most noticeable effect under weak coupling conditions. If simulations of QCL dynamics for these system parameters are carried out using a mapping hamiltonian basis, the results are indistinguishable from exact quantum dynamics [40]. This again suggests that the small discrepancies are due to the use of the momentum-jump approximation.

The asymmetric spin boson model presents a significantly more challenging non-adiabatic condensed phase test problem due to the asymmetry in forces from the different surfaces. Approximate mean field methods, for example, will fail to reliably capture the effects of these different forces on the dynamics.

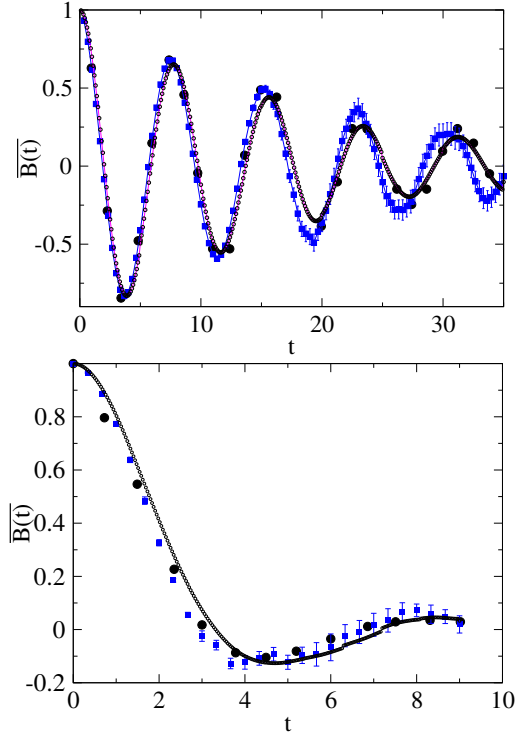


Fig. 1: Plots of $\bar{B}(t) = \text{population difference} = \langle \sigma_z \rangle(t)$ for the symmetric spin-boson ($\epsilon = 0$) as functions of time: Exact quantum results from Ref. [41] (solid circles), TQCL algorithm (squares), ILDM propagation (open circles). Upper panel presents results for low temperature, weak system-bath coupling case: $\beta = 12.5$, $\xi = 0.09$ and $\Omega = 0.4$. Lower panel presents exact quantum results from Ref. [42] (solid circles), TQCL algorithm (squares), and ILDM propagation (open circles) for intermediate temperature and strong system-bath coupling: $\beta = 3$, $\xi = 0.5$ and $\Omega = 0.333$.

In Fig. 2 we compare results using $\epsilon = 0.4$ for the two mixed quantum-classical methods outlined in this chapter with exact results obtained from MCTDH wavepacket dynamics calculations. To make a reliable comparison the approximate finite temperature calculations were performed at very low temperatures ($\beta = 25$), though a product of ground state wave functions for the independent harmonic oscillator modes could have been used to make the initial conditions identical to those used in the MCTDH calculations.

From the upper panel in Fig. 2 we see that both the ILDM, and TQCL results reproduce those obtained from MCTDH wavepacket propagation. The ILDM calculations were run with 2 attempted hops per time unit and results

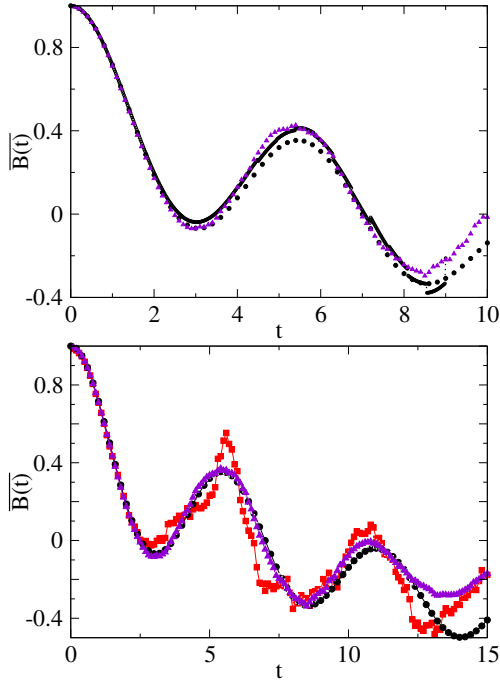


Fig. 2: $\bar{B}(t) = \langle \sigma_z \rangle(t)$ versus time for the asymmetric spin-boson model with $\beta = 25$, $\xi = 0.13$ and $\Omega = 0.4$, $\epsilon = 0.4$. (Top) Comparison of exact quantum results (filled circles), ILDM simulations (small open circles), and QCL dynamics (filled triangles). Both ILDM and QCL simulations were carried out for an ensemble of 2×10^6 trajectories and no filters are employed. (Bottom) Convergence of TQCL dynamics with ensemble size: 2×10^4 (filled squares) and 1×10^6 (filled triangles). Exact quantum results (filled circles). A filter parameter of $Z = 500$ is used for these calculations .

are presented for an ensemble of $\mathcal{N} = 2 \times 10^6$ trajectories. Beyond this time, without using a filtering approach the statistical noise in the ILDM calculations becomes overwhelming. Convergence with ensemble size for the TQCL approach using a small value of the filter cutoff ($Z=500$) is explored in the other curves presented in the lower panel.

The nature of the quantum coherent dynamics in the system can be investigated by computing the off-diagonal elements of the quantum subsystem density matrix obtained by tracing over the bath degrees of freedom, $\rho_{12}(t) = \int dRdP \rho_{12}(R, P, t)$. The time dependence of the real and imaginary parts of $\rho_{12}(t)$ are shown in Fig. 3. The off-diagonal elements of the reduced density matrix computed with the two different mixed quantum classical ap-

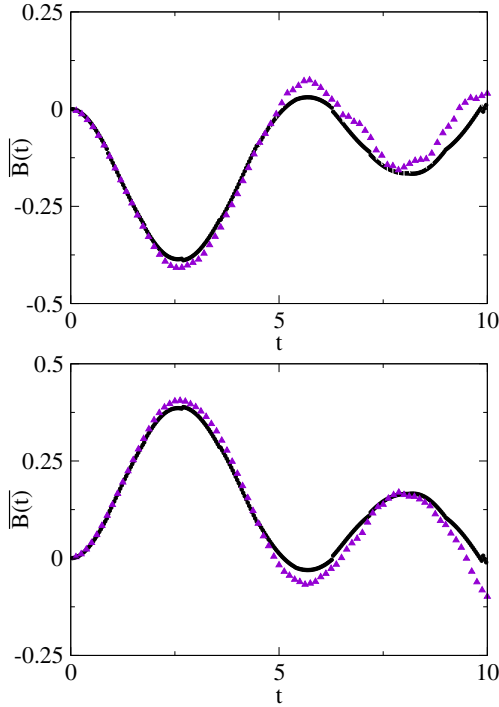


Fig. 3: Real (top) and imaginary (bottom) parts of $\rho_{12}(t)$ versus time for the same system parameters as in Fig. 2. Small circles, ILDM simulations; triangles, QCL dynamics. In both cases 10^6 trajectories were used to obtain the results.

proaches agree to within the statistical uncertainty of the calculations. One of the important properties of these methods that distinguishes them from many other mixed quantum classical approaches is their ability to treat these coherence terms with out making *ad hoc* approximations. Traditional surface hopping trajectory approaches [1, 3], for example, either completely neglect decoherence, or incorporate its effects by damping out off-diagonal elements of the reduced density matrix with some phenomenological exponential decoherence time. In contrast, both the QCL and ILDM propagation schemes include decoherence effects in a completely *ab initio* fashion by accumulating interfering contributions to the off-diagonal density matrix elements over the ensemble of phase factor weighted trajectories. In general the reliable computation of such interference effects is numerically intensive as large ensembles are required to accurately add the interfering contributions. The results in Fig. 3 for the asymmetric spin-boson system considered here show long lived coherent oscillation of the off-diagonal elements for these conditions, with

no evidence of exponential decay assumed in the phenomenological models of condensed phase decoherence processes. The dephasing is at least as long lived as the population relaxation dynamics for this model system.

5 Conclusion

The two quantum-classical dynamical schemes discussed in this Chapter provide ways to investigate the dynamics of large, many-body systems where quantum degrees of freedom are coupled to an environment. The results presented here have shown that both schemes yield good agreement with exact calculations for the symmetric and asymmetric spin-boson models for a wide range of system parameters. In particular coherences are accurately described. Our simulation results have documented the performances of the algorithms with respect to quantities such as the number of trajectories in the ensemble needed to obtain good results, the use of filters and the utility of the momentum-jump approximation. The QCL formulation can be shown to be exact for the spin-boson model so our comparison with numerically exact results for this model tests only the approximations in the implementation scheme. Calculations on models for which this formulation is not exact would offer more challenging tests and may provide a more stringent basis for comparing the different methods in future studies.

While the two methods are, at face value, quite different in the ways in which full quantum dynamics is reduced to quantum-classical dynamics, there are common elements in the manner in which they are simulated. The Trotter-based scheme for QCL dynamics makes use of the adiabatic basis and is based on surface-hopping trajectories where transitions are sampled by a Monte Carlo scheme that requires reweighting. Similarly, ILDM calculations make use of the mapping hamiltonian basis and also involve a similar Monte Carlo sampling with reweighting of trajectories in the ensemble used to obtain the expectation values of quantum operators.

As noted above, however, the theoretical frameworks of the two approaches appear quite different. This is a common situation in mixed quantum-classical simulations: many methods exist, and they may have very different ranges of applicability. A systematic assessment of differences and similarities, of the accuracy of various approximations, and in general of their relative merits presents a significant challenge. Investigating the relationships between different methods, however, can provide a better understanding of the nature, advantages and limitations of mixed quantum-classical methods in general, and may lead to a more firm theoretical foundation on which to base the development of new methods, as well as more efficient algorithms for implementation.

The two methods described in this Chapter are good candidates for such comparative investigation. They are both derived employing well-defined approximations to exact quantum expressions and they can be used to study

the same set of, general, observables. Furthermore, it has already been shown that, for some choices of the quantum sub-system basis set, QCL can be obtained via a linearization procedure that shares some similarities with the linearization used to derive the ILDM propagation [4]. Future work will investigate the theoretical connections between the methods that, as a first step, we have compared in their existing formulations in this Chapter.

Acknowledgements

The research of RK was supported in part by a grant from the Natural Sciences and Engineering Research Council of Canada. DFC acknowledges support for this research from the US National Science Foundation under grant number CHE-0616952, as well as his Stokes Professorship from Science Foundation Ireland, and funding from University College Dublin. A grant from Ministero dell’Ambiente e della Tutela del Territorio e del Mare is acknowledged by SB and GC.

References

1. Tully JC. Mixed quantum-classical dynamics: mean-field and surface-hopping. In *Classical and Quantum Dynamics in Condensed Phase Simulations*, ed. B.J. Berne, G. Ciccotti, D.F. Coker. Chapter 21. Singapore: World Scientific, 1998.
2. For a review with references to the literature on this topic, see, R. Kapral. Progress in the theory of mixed quantum-classical dynamics. *Annu. Rev. Phys. Chem.*, 57:129, 2006.
3. J. C. Tully. Molecular dynamics with electronic transitions. *J. Chem. Phys.*, 93(2):1061, 1990.
4. Q. Shi and E. Geva. A derivation of the mixed quantum-classical Liouville equation from the influence functional formalism. *J. Chem. Phys.*, 121(8):3393, 2004.
5. S. Nielsen, R. Kapral, and G. Ciccotti. Statistical mechanics of quantum-classical systems. *J. Chem. Phys.*, 115(13):5805, 2001.
6. H. Kim and R. Kapral. Transport properties of quantum-classical systems. *J. Chem. Phys.*, 122:214105, 2005.
7. G. Ciccotti, D.F. Coker, and R. Kapral, *Quantum statistical dynamics with trajectories*, in *Quantum dynamics of complex molecular systems*, David Micha and Irene Burghardt, Chemical Physics series vol. 83, (Springer, Berlin), p. 275, 2006.
8. H. Kim and R. Kapral. Nonadiabatic quantum-classical reaction rates with quantum equilibrium structure. *J. Chem. Phys.*, 123:194108, 2005.
9. R. Grunwald, H. Kim and R. Kapral. Surface hopping and decoherence with quantum equilibrium structure. *J. Chem. Phys.*, 128:164110, 2008.
10. G. Hanna and R. Kapral. Quantum-classical Liouville dynamics of nonadiabatic proton transfer. *J. Chem. Phys.*, 122(24):244505, 2005.

11. G. Hanna and R. Kapral. Quantum-classical Liouville dynamics of proton and deuteron transfer rates in a hydrogen bonded complex. *J. Chem. Phys.*, 128:164520, 2008.
12. R. Kapral and G. Ciccotti. Mixed quantum-classical dynamics. *J. Chem. Phys.*, 110:8919, 1999.
13. I. V. Aleksandrov. The statistical dynamics of a system consisting of a classical and a quantum subsystem. *Z. Naturforsch.*, 36:902, 1981.
14. V. I. Gerasimenko. Correlation-less equations of motion of quantum-classical systems. *Repts. Acad. Sci. Ukr.SSR*, (10):64, 1981.
15. V. I. Gerasimenko. Dynamical equations of quantum-classical systems. *Theor. Math. Phys.*, 50:49, 1982.
16. W. Boucher and J. Traschen. Semiclassical physics and quantum fluctuations. *Phys. Rev. D*, 37(12):3522, 1988.
17. W.Y. Zhang and R. Balescu. Statistical mechanics of a spin polarized plasma. *J. Plasma Physics*, 40:199, 1988.
18. Y. Tanimura and S. Mukamel. Multistate quantum Fokker–Planck approach to nonadiabatic wave packet dynamics in pump–probe spectroscopy. *J. Chem. Phys.*, 101:3049, 1994.
19. C. C. Martens and J. Y. Fang. Semiclassical-limit molecular dynamics on multiple electronic surfaces. *J. Chem. Phys.*, 106(12):4918, 1997.
20. I. Horenko, C. Salzmann, B. Schmidt, and C. Schutte. Quantum-classical liouville approach to molecular dynamics: Surface hopping gaussian phase-space packets. *J. Chem. Phys.*, 117(24):11075, 2002.
21. R. Grunwald, A. Kelly and R. Kapral. Quantum dynamics in almost classical environments. *this volume*, 2009.
22. D. Mac Kernan, G. Ciccotti, and R. Kapral. Trotter-based simulation of quantum-classical dynamics. *J. Phys. Chem. B*, 112:424, 2008.
23. R. Kapral and G. Ciccotti, *A Statistical Mechanical Theory of Quantum Dynamics in Classical Environments*, in *Bridging Time Scales: Molecular Simulations for the Next Decade*, eds. P. Nielaba, M. Mareschal, G. Ciccotti, (Springer, Berlin), p. 445, 2002.
24. R. Hernandez and G. Voth. Quantum time correlation functions and classical coherence. *Chem. Phys.*, 223:243, 1998.
25. J.A. Poulsen and G. Nyman and P.J. Rossky. Practical evaluation of condensed phase quantum correlation functions: A Feynman-Kleinert variational linearized path integral method. *J. Chem. Phys.*, 119:12179, 2003.
26. Q. Shi and E. Geva. Vibrational energy relaxation in liquid oxygen from a semiclassical molecular dynamics simulation. *J. Phys. Chem. A*, 107:9070, 2003.
27. Q. Shi and E. Geva. Semiclassical theory of vibrational energy relaxation in the condensed Phase. *J. Phys. Chem. A*, 107:9059, 2003.
28. Q. Shi and E. Geva. Nonradiative electronic relaxation rate constants from approximations based on linearizing the path-integral forward-backward action. *J. Phys. Chem. A*, 108:6109, 2004.
29. X. Sun and W.H. Miller. Semiclassical initial value representation for electronically nonadiabatic molecular dynamics. *J. Chem. Phys.*, 106:6346, 1997.
30. G. Stock and M. Thoss. Semiclassical description of nonadiabatic quantum dynamics. *Phys. Rev. Lett.*, 78:578, 1997.
31. G. Stock and M. Thoss. Mapping approach to the semiclassical description of nonadiabatic quantum dynamics. *Phys. Rev. A*, 59:64, 1999.

32. S. Bonella and D.F. Coker. A semi-classical limit for the mapping Hamiltonian approach to electronically non-adiabatic dynamics. *J. Chem. Phys.*, 114:7778, 2001.
33. S. Bonella and D.F. Coker. Semi-classical implementation of the mapping Hamiltonian approach for non-adiabatic dynamics: Focused initial distribution sampling. *J. Chem. Phys.*, 118:4370, 2003.
34. S. Bonella and D.F. Coker. LAND-map, a linearized approach to nonadiabatic dynamics using the mapping formalism. *J. Chem. Phys.*, 122:194102, 2005.
35. S. Bonella, D. Montemayor, and D.F. Coker. Linearized path integral approach for calculating nonadiabatic time correlation functions. *Proc. Natl. Acad. Sci.*, 102:6715, 2005.
36. D.F. Coker and S. Bonella, *Linearized path integral methods for quantum time correlation functions*, in *Computer simulations in condensed matter: From materials to chemical biology*, eds. M. Ferrario and G. Ciccotti and K. Binder, Lecture Notes in Physics 703, (Springer-Verlag, Berlin), p. 553, 2006.
37. E. Dunkel, S. Bonella, and D.F. Coker. Iterative linearized approach to non-adiabatic dynamics. *J. Chem. Phys.*, 129:114106, 2008.
38. Z. Ma and D.F. Coker. Quantum initial condition sampling for linearized density matrix dynamics: Vibrational pure dephasing of iodine in krypton matrices. *J. Chem. Phys.*, 128:244108, 2008.
39. D. Mac Kernan, G. Ciccotti, and R. Kapral. Surface-hopping dynamics of a spin-boson system. *J. Chem. Phys.*, 116(6):2346, 2002.
40. H. Kim, A. Nassimi, and R. Kapral. Quantum-classical Liouville dynamics in the mapping basis. *J. Chem. Phys.*, 129:084102, 2008.
41. D. E. Makarov and N. Makri, *Chem. Phys. Lett.*, 221:482, 1994.
42. K. Thompson and N. Makri. Rigorous forward-backward semiclassical formulation of many-body dynamics. *Phys. Rev. E*, 59(5):R4729, 1999.